Optik 126 (2015) 4910–4915

Contents lists available at ScienceDirect

Optik

journal homepage: www.elsevier.de/ijleo

A new robust 2D camera calibration method using RANSAC

Yaowen Lv [a], Jinliang Feng [a,*], Zhaokun Li [b], Wei Liu [b], Jingtai Cao [b,c]

[a] School of Optoelectronic Engineering, Changchun University of Science and Technology, 7089 Weixing Road, Changchun 130022, Jilin, PR China
[b] College of Communication Engineering, Jilin University, 5372 Nanhu Road, Changchun 130012, PR China
[c] Changchun Institute of Optics, Fine Mechanics and Physics, Chinese Academy of Sciences, 3888 Nanhu Road, Changchun 130033, PR China

ARTICLE INFO

Article history:
Received 3 November 2014
Accepted 11 September 2015

Keywords:
Camera calibration
RANSAC
Machine vision

ABSTRACT

Camera calibration is a basic and crucial problem in computer vision and photogrammetry. The traditional calibration approach based on 2D planar target fails to give reliable and accurate results due to the inaccurate localization of feature points in some calibration images. An accurate and robust estimation method for camera parameters based on RANdom SAmple Consensus (RANSAC) algorithm is proposed to exclude the unreliable images in this study. First, the distance between circular point and image of the absolute conic is defined, and the recommended threshold value is given by computer simulation. Second, RANSAC has been utilized to pick out a subset of calibrating images automatically, and linear algebraic approximation is performed to estimate the intrinsic parameters and external parameters. Finally, all the camera parameters including lens distortion parameters are refined by the non-linear searching algorithm. Numerical simulation and practical experiment in this paper demonstrate the accuracy and robustness of the proposed method. The experimental results show that the proposed method is more robust and efficient in improving the calibration accuracy than the traditional methods.

1. Introduction

Camera calibration, whose applications include 3D reconstruction, visual inspection, object localization [1], camera localization [2] and robot navigation, etc, is essential to computer vision. Tsai [3] gave a comprehensive survey of the problem. Two kinds of parameters should be considered in the model. The intrinsic parameter set, which models the internal geometry and optical characteristics of the image sensor, determines how light is projected through the lens into the image plane of the sensor. The other one, the extrinsic parameters, measure the position and orientation of the camera in the world coordinate system, it provides metric information with respect to a user-fixed coordinate system instead of the camera coordinate system. For applications with strict requirement of accuracy, lens distortions [4–6] should be taken into account.

Camera calibration has received increased attention during the past two decades. Various effective algorithms have been reported, according to the calibration object, they are divided into two classes: self-calibration and object based calibration.

1.1. Self-calibration

Camera calibration is performed by moving a camera around an unknown static scene. Only a few corresponding points in multi-images are sufficient to calibrate the intrinsic parameters of a camera [7–9]. The main idea is to find the camera parameters that satisfy the pairwise epipolar constraints, and the Kruppa equations are derived for self-calibration. Other self-calibration techniques based on vanishing points are also introduced [10,11]. However, there are three significant limitation of self-calibration: (1) Sufficient correspondences between views must be established, which is impossible when the scene is featureless. (2) Solving Kruppa equation is difficult and not reliable in practice. (3) Lens distortions are not considered in almost all existing self-calibration papers, so the calibration accuracy is not good enough for photogrammetric applications.

1.2. Object based calibration

Initially, 3D calibration object [1,7] is used for camera calibration, in which the 3D points and their 2D projections are associated with a projection matrix. The perspective projection formulations can be obtained linearly from only one image. It requires an expensive calibration apparatus and elaborate setup. To overcome this shortcoming, new technique bases on 2D patterns have

* Corresponding author. Tel.: +86 43185582533.
E-mail address: fengjinliangcust@163.com (J. Feng).

http://dx.doi.org/10.1016/j.ijleo.2015.09.117
0030-4026/

been proposed in latter literature [12,13]. Most recently, Zhang [14] proposed a calibration using 1D pattern (points aligned on a line), that has been investigated and extended by several other authors [15–17]. The main advantage of using 1D patterns to make the calibration is the possibility to calibrate several cameras at the same time, because the points of the 1D pattern can be visible simultaneously by multiple cameras even apart from each other.

Among the existing camera calibration techniques, Zhang's method [12], which is used as the basis of Bouguet's camera calibration toolbox in Matlab [18] and OpenCV [19], is flexible by observing a planar target for at least twice, the main idea is to obtain the camera parameters from the homography between 2D object plane and the corresponding image plane. Due to their ease of use, calibration algorithms that use planar patterns have gained widespread acceptance [20–22]. Recently, the technique mainly focuses on the following three aspects: (1) Feather detection and localization. Jun Chu [23] proposed a novel chessboard corners detection which is based on morphological dilation and round template. This algorithm provides an effective and automatic mechanism for chessboard corners detection and can be used in complex scene. A quick and robust detection of chessboard features is also proposed by Stuart Bennett and Joan Lasenby [24]. The Chess-board Extraction by Subtraction and Summation (ChESS) feature detector is designed to exclusively respond to chessboard corners. In addition to chessboard planer pattern, circle and ring patterns have also been utilized [13,25–27]. To improve the accuracy of the control points, an iterative refinement approach has been introduced and evaluated [28]. (2) Novel optimization method. Fuqiang Zhou [29] proposed a novel optimization method of camera parameters by minimizing the metric distance between actual and computed object points in camera coordinate system instead of the difference between the detected image point and the projected image point calculated by camera parameters. Fuqiang Zhou [30] developed a planer-based technique, in which RANSAC algorithm is used to refine the calibration parameters. (3) Optimal setting for accurate calibration. The effect of the illumination intensity, the number of control points, the region of interest and 2D plane position on improving the accuracy and repeatability of calibration have been investigated [31,32].

It is easy for us to take abundant images (more than 20 images) when Zhang's method [12] is used for off-line camera calibration. However, it is well-known that it is difficult to accurately and reliably extract all wanted features in all images in the presence of noise, occlusion, image blur, and changing illumination or viewpoint. When different subsets of images are selected to calibrate a camera, the calibration result will not converge because of inaccurate features detection. Therefore, to gain reliable and accurate calibration parameters, it is an extremely important task for us to detect and remove the unreliable images. In this paper, a novel calibration method is proposed to cope with this problem. Our proposed detection method works as following three steps: First, Random Sample Consensus (RANSAC) algorithm is employed to select a subset of calibrating images automatically. Second, linear algebraic approximation is performed to estimate the intrinsic parameters and external parameters. Finally, all the camera parameters including lens distortion parameters are refined by Levenberg–Marquardt algorithm. To the best of our knowledge, there is little report about using RANSAC in Zhang's method except [30], in which RANSAC method is utilized to remove the unreliable corresponding points after non- linear searching. However, since camera parameters are coupled, nonlinear searching performs badly and local solution is reached frequently, Zhou's method is limited and mainly depends on the initialization. Compared with existing camera calibration techniques, the advantages of our method are: (1) It requires no prior known knowledge about the positions and orientations from where images should be taken. (2) The subset of images is selected automatically, so the proposed method can be utilized by general public even who are not experts in computer vision. (3) The camera parameters need only to be one-off optimized by nonlinear searching.

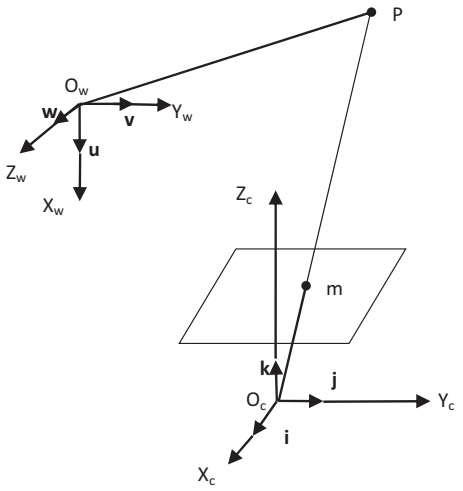

Fig. 1. Pinhole camera model.

The paper is organized as follows: Section 2 describes the preliminary knowledge in this paper, including Zhang's 2D calibration method and the principle of RANSAC. The details of the proposed calibration algorithm are depicted in Section 3. Section 4 provides the experimental results. Both computer simulation and real data are used to validate the proposed technique. Finally, Section 5 concludes the paper with perspective of this work.

2. Preliminaries

2.1. Camera model

The classical pinhole camera model is shown in Fig. 1. Oc-XcYcZc is the coordinate system of camera, Oc is the optical center of camera, the coordinate axes OcXc and OcYc are, respectively, parallel to the rows and columns of the image plane, OcZc is the optical axis of camera. The unit vectors of are three coordinate axes, respectively: $\boldsymbol{i}$, $\boldsymbol{j}$, $\boldsymbol{k}$. O_w–$X_wY_wZ_w$ is the built World Coordinate System (WCS), $\boldsymbol{u}$, $\boldsymbol{v}$, $\boldsymbol{w}$ are the unit vectors of the coordinate axes of WCS. If the translation vector from WCS to the camera coordinate system is $\boldsymbol{t}$, the rotation matrix is $\mathbf{R}$. $\boldsymbol{t}$ is the representation of the origin O_w of WCS in camera coordinate system.

In this model, any point P in the space and its projection m on camera image plane satisfy the projection formula below:

$$s\begin{bmatrix} u \\ v \\ 1 \end{bmatrix} = \mathbf{K}[\mathbf{R}\cdot\boldsymbol{t}]\begin{bmatrix} x \\ y \\ z \\ 1 \end{bmatrix} \quad \text{with} \quad \mathbf{K} = \begin{bmatrix} f_x & 0 & u_o \\ 0 & f_y & v_o \\ 0 & 0 & 1 \end{bmatrix} \tag{1}$$

where (u, v) is the image coordinate of projective point m, (x,y,z) is the three-dimensional coordinate of P in WCS, $\mathbf{K}$ is the matrix of camera intrinsic parameters, consisting of four parameters: the scaling factors f_x and f_y in horizontal and vertical direction, respectively, the optical axis centre (u_o, v_o). $\mathbf{R}$, $\boldsymbol{t}$ are, respectively, the rotation matrix and translation vector from WCS to camera coordinate system.

2.2. Lens distortion model

In practice, real lens do not satisfy the ideal pin-hole model, the lens distortions of the consumer-grade digital cameras cannot

Table 1
External parameters for nine model planes.

Homography	Rotation vector (rad)	Translation vector (mm)
H1	(1.65,1.65,−0.67)	(−182.18,−82.39,858)
H2	(1.84,1.89,−0.40)	(−159.1,−158.05,763.11)
H3	(1.74,2.07,−0.51)	(−129.43,−173.25,781.13)
H4	(1.83,2.11,−1.10)	(−68.71,−153.57,784.27)
H5	(1.08,1.92,−0.25)	(−96.47,−227.88,742.4)
H6	(−1.70,−1.93,−0.80)	(−151.32,−78.85,448.24)
H7	(1.99,1.93,1.31)	(−85.49,−77.11,445.39)
H8	(1.96,1.82,1.33)	(−173.31,−102.99,467.94)
H9	(−1.37,−1.99,0.32)	(−5.7435,−224.23,−735.45)

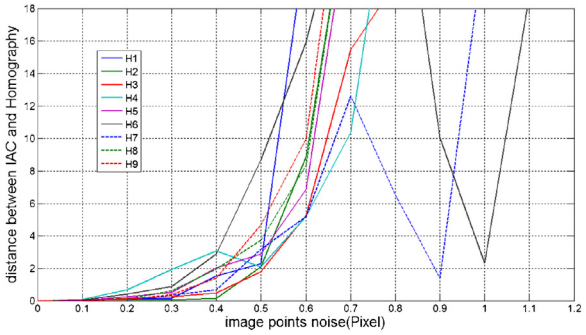

Fig. 2. Distance between IAC and homography with respect to noise level.

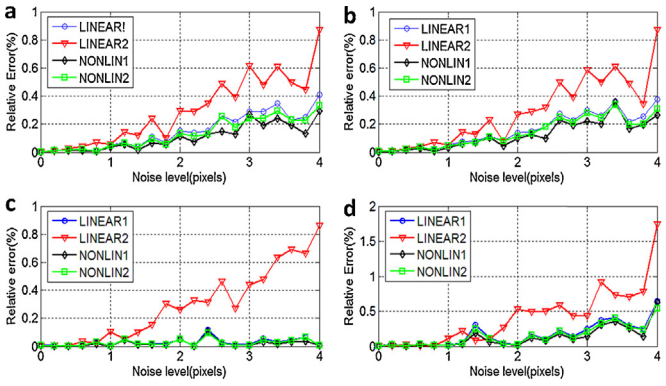

Fig. 3. Relative error with respect to noise level: (a) f_x; (b) f_y; (c) u_o; (d) v_o.

be ignored. Thus, a proper distortion model should be selected. The most commonly used method proposed by Brown [33] is to decompose the distortion into radial, decentering, and prism components. Radial distortion is caused by flawed radial curvature of the lens elements. Decentering distortion is due to non-strict coaxiality [4,34] of the optical centers of lens elements. Thin prism distortion arises from the imperfection in lens design and manufacturing as well as camera assembly. In general, the radial distortion is sufficient for a high-accuracy measurement since no more elaborated model improve the accuracy significantly [5,6]. The model for correcting the radial distortion is given:

$$u_d = u + k_1(u - u_0)r^2$$
$$v_d = v + k_1(v - v_0)r^2 \tag{2}$$

where $r^2 = x_n^2 + y_n^2$, (x_n, y_n) is the ideal normalized image coordinates, (u, v) is the corrected image point and (u_d, v_d) is the corresponding image point with radial distortion, k_1 is the coefficients of the radial distortion.

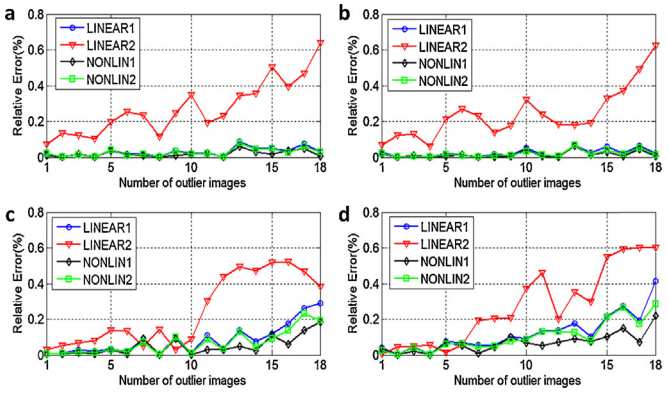

Fig. 4. Relative error with respect to the number of outlier images: (a) f_x; (b) f_y; (c) u_o; (d) v_o.

2.3. RANSAC

RANdom SAmple Consensus (RANSAC) was first published by Fischler and Bolles [35]. RANSAC algorithm is often used in computer vision, e.g., to simultaneously solve the correspondence problem, and estimate the fundamental matrix related to a pair of stereo cameras [7,36]. It is an iterative method to estimate parameters of a mathematical model from a set of observed data which contains outliers. Standard RANSAC algorithm proceeds as follows: (1) A minimal subset of the input data is randomly selected and model parameters fitting these data are computed. (2) All other data are tested against the fitted model and the support data is selected as consensus set for this model. (3) The model parameters are estimated from the consensus set. This procedure is repeated a fixed number of iterations, each time producing either a model which is rejected because too few points are part of the consensus set, or a refined model together with a corresponding consensus set size. In the latter case, we keep the refined model if its consensus set is larger than the previously saved model. The consensus set for each iteration is determined from specific requirements related to the application. This problem will be further discussed in Section 3. The number of iterations can be determined from probability theory. Let p be the probability that the RANSAC algorithm selects only inliers from the input data set in some iteration. The number of iterations is governed by an expression of the following form [7,35]:

$$k = \frac{\log(1-p)}{\log(1-w^n)} \tag{3}$$

where w is the proportion of inliers and n is the size of the minimal subset from which the model parameters are estimated. A common case is that w is not well known beforehand. An adaptive algorithm is introduced to determine the number of iterations. This adaptive is fully described in Ref. [7]. This adaptive approach works very well and in practice covers the questions of both the number of samples and terminating the algorithm. This adaptive algorithm is implemented by Peter Kovesi [37] and some examples are also given.

3. Camera calibration with RANSAC

According to Zhang's method [12], given an image of the planar calibration pattern, a homography can be estimated and two basic constraints on the intrinsic parameters can be given:

$$\boldsymbol{h}_1^T \boldsymbol{K}^{-T} \boldsymbol{K}^{-1} \boldsymbol{h}_2 = 0$$
$$\boldsymbol{h}_1^T \boldsymbol{K}^{-T} \boldsymbol{K}^{-1} \boldsymbol{h}_1 = \boldsymbol{h}_2^T \boldsymbol{K}^{-T} \boldsymbol{K}^{-1} \boldsymbol{h}_2 \tag{4}$$

where $\boldsymbol{h}$ is the row of the homography between the points on the pre-known plane pattern and the corresponding image points. If m images of planar calibration are taken, m equations such as Eq. (4) arise. At least two images are necessary to obtain a unique solution. The close-form solution can be estimated simply by Singular Value Decomposition (SVD). Once $\boldsymbol{K}$ is known, extrinsic parameters for each image are computed when the corresponding homography is known (see [12] for details). This closed form solution is crucial to avoid divergences to local solution with the nonlinear searching. In practice, it is difficult to accurately and reliably extract all wanted features in all images in the presence of noise, occlusion, image blur, and changing illumination or viewpoint, etc. This means that the unreliable images will lead to inaccurate camera parameters if they are involved in the calibration process. Therefore, it is important for us to exclude the unreliable images. RANSAC is performed to focus on the problem. As mentioned, to calibrate the pinhole camera model, two minimal data for random sampling are needed. Subsequently, the linear algorithm is adopted to calculate the image of the absolute conic (IAC), described by $\boldsymbol{K}^{-\boldsymbol{T}}\boldsymbol{K}^{-1}$ [7]. If the circular point, defined by homography, is exactly on the IAC, Eq. (4) is satisfied. Thus, the distance between the circular point and the IAC means the accuracy of camera intrinsic parameters. The distance is defined as following form:

$$\begin{aligned} d &= \frac{\left(\boldsymbol{h}_1^{\boldsymbol{T}}\boldsymbol{B}\boldsymbol{h}_2\right)^2}{\boldsymbol{B}\boldsymbol{h}_2(1)^2+\boldsymbol{B}\boldsymbol{h}_2(2)^2+\boldsymbol{B}\boldsymbol{h}_1(1)^2+\boldsymbol{B}\boldsymbol{h}_1(2)^2} \\ &\quad + \frac{\left(\boldsymbol{h}_3^{\boldsymbol{T}}\boldsymbol{B}\boldsymbol{h}_4\right)^2}{\boldsymbol{B}\boldsymbol{h}_3(1)^2+\boldsymbol{B}\boldsymbol{h}_3(2)^2+\boldsymbol{B}\boldsymbol{h}_4(1)^2+\boldsymbol{B}\boldsymbol{h}_4(2)^2} \\ \boldsymbol{h}_3 &= \boldsymbol{h}_1-\boldsymbol{h}_2 \\ \boldsymbol{h}_4 &= \boldsymbol{h}_1+\boldsymbol{h}_2 \end{aligned} \tag{5}$$

where $\boldsymbol{B}$ is the matrix of IAC, which satisfies: $\boldsymbol{B}=\boldsymbol{K}^{-\boldsymbol{T}}\boldsymbol{K}^{-1}$, $\boldsymbol{h}_i(i=1, 2)$ is the row i of the homography and $\boldsymbol{B}\boldsymbol{h}(j)(j=1, 2)$ represents the element j of vector $\boldsymbol{B}\boldsymbol{h}$.

When the distance is calculated, the last problem is to choose the distance threshold t. If the distance between the circular point and the IAC is larger than t, the corresponding image is identified as outlier and will be removed in the next step. It is difficult for us to choose the distance threshold t. A very high threshold may mistakenly classify the outliers into the consensus set while a very low threshold may cause instability in some case because the measurement of image coordinates is inexact (generally termed noise). In this paper, the threshold value is recommended by computer simulation in Section 4.1.1.

To sum up, the recommended plane calibration procedure with RANSAC is described as follows:

(1) Take abundant images (more than 20 images) of the model plane under different orientations by moving the model plane;
(2) Extract the feature points in the images and compute the homography matrix for each image [7,18];
(3) Set parameters for adaptive RANSAC method: $s=2$, $w=0$, $k=\infty$, $t=1$, $i=1$;
(4) Randomly select two homography matrixes and estimate the IAC according to Eq. (4);
(5) Identify a set of inliers consistent with the evaluated IAC according to Eq. (5) and the threshold value t;
(6) Update the sample count value k by Eq. (3), if a larger consistent is found;
(7) If $i>k$, the largest consensus set is acquired, go to step (8); else $i=i+1$, go to step (4);
(8) Once the largest consensus is obtained, the subset of calibrating images is determined. Then the camera parameters are calculated by Zhang's method.

4. Experiment results

The proposed algorithm discussed in this paper is analyzed using both synthetic and real data. It is considered that the noise presented in the data follows a normal distribution with mean value 0 and standard deviations δ. The experiments executed for each data type are described in the following.

4.1. Computer simulations

The synthetic data are generated by assuming a camera with the following parameters: $k_x=662.64$; $k_y=664.91$; $u_0=306.89$; $v_0=241.45$. The image resolution is 640×480 pixel. The lens distortion parameter is 0. The model plane is a chessboard pattern containing $12\times12=144$ corner points. The size of pattern is 30 mm × 30 mm. The orientation of the plane is represented by a 3D vector $\boldsymbol{r}$, which is the Rodrigues notation of rotation matrix from world coordinate system to camera coordinate system. Its position is determined by a 3D translation vector $\boldsymbol{t}$.

4.1.1. Determining the recommended threshold value t

In this experiment, we use nine planes with the external parameters presented in Table 1. Noise is added to the projected image points with δ ranging from 0.1 to 1.2 pixel. We compute the distance between the homography and IAC, respectively. For each noise level, 500 independent trials are performed, the average results are shown in Fig. 2. From Fig. 2, the distance varies linearly when the noise level is less than 0.3 pixel. As the noise level growth continues, it is sharply increases while the noise of projected image points is greater than 0.4 pixel. That is to say, calibration will be not performed accurately when the precision of locating image points is less than 0.4 pixel. In real vision measurement system, the error of locating image points in image is less than 0.2 pixel [38]. Therefore, the distance threshold value is obtained as $t=1$. This threshold value will be utilized in the following experiments.

4.1.2. The proposed method testing with synthetic data

In this work, four methods were analyzed: (1) the linear method with RANSAC proposed in the present article and called LINEAR1; (2) the linear method proposed by Zhang [12]; (3) The method that refines the estimation of LINEAR1 through the Levenberg–Marquardt algorithm called NONLIN1; (4) The method that refines the estimation of LINEAR2 through the Levenberg–Marquardt algorithm called NONLIN2. Two individual experimental are conducted. One experimental tests the calibration accuracy relative to the input noise level and the other tests the calibration accuracy relative to the number of outlier images.

In Test 1, fifteen calibration images are created. The orientation and position of the model plane for the first nine images are the same as the last Section 4.1.1. From the tenth images, we first randomly choose a rotation axis in a uniform sphere, then apply a rotation angle of 25°. Gaussian noise with mean value 0 and standard deviation δ is added to the image points, where δ is varied from 0 to 4 pixel with the step length of 0.2 pixel. The calibrated parameters are compared with the ground truths and their relative errors are measured. For each input noise level, 100 independent trials are performed. The average results are shown in Fig. 3.

In the other test, twenty calibration images are generated with the similar method in Test 1. We divide the calibration images into two parts: inlier images and outlier images. The noise of inlier images is set as 0.2 pixel (which is the noise level in the practical calibration). The noise of outlier images is set as 3 pixel. The number of outlier images varies from 1 to 18. For each number, the outlier images are chosen randomly. 100 independent trials are conducted. The accuracy of the calibrated parameters is measured in the same

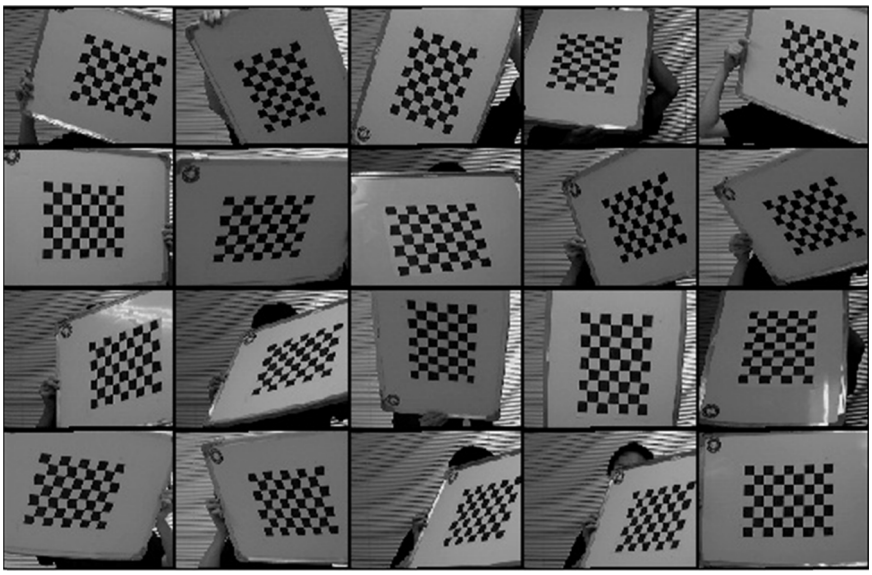

Fig. 5. Twenty images of a model plane.

Table 2
Comparative results of camera parameters and calibration accuracy.

Method	f_x (pixel)	f_y (pixel)	u_o (pixel)	v_o (pixel)	k_1 (mm^{-2})	Err (pixel)	Iteration number
LINEAR1	2542.21	2497.65	354.18	210.45	–	2.046	–
LINEAR2	2490.65	2790.29	294.43	208.28	–	0.365	–
NONLIN1	2462.09	2628.63	305.63	220.94	−0.610	0.131	3
NONLIN2	2456.09	2620.26	307.57	208.58	−0.586	0.213	18

way as in Test 1. Fig. 4 shows the mean value of the relative error of the intrinsic parameters.

It can be seen from the results shown in Figs. 3 and 4 that the accuracy of the LINEAR1 method is significantly higher than LINEAR2. In addition, Levenberg–Marquardt refines the estimations of both linear methods. The LINEAR1 method proposed in this paper provides initial parameters values which are very close to the global minimum. For that reason, in Figs. 3 and 4, the curves corresponding to the LINEAR1 and nonlinear methods are almost overlapping. In the present work, convergence occurred in only three iterations. Thus, according to the required accuracy, this refinement does not even need to be executed on some occasions. From the results shown in Fig. 4, it can be seen that the error caused by the proposed RANSAC method (LINEAR1 and NONLIN1) keeps in a very low level which demonstrates the robustness to the outlier images.

The two experiments on synthetic data demonstrate that the proposed calibration algorithm not only can produce very high accuracy on intrinsic parameters under the standard input noise level, but also can be robust to the outlier images.

4.2. Real data

Since the ground truths of camera parameters are not available in the experiments for real data, it is necessary to take appropriate methods to evaluate accuracy in terms of camera parameters. Four of the most frequently used methods were adopted [5,30]: the error of distorted pixel coordinates, the error of undistorted pixel coordinates, the distance with respect to the optical ray, and normalized calibration error. In the present work, we just calculate the error of distorted pixel coordinates to evaluate our calibration accuracy. This is because Salvi [5] has pointed out that good calibrating algorithms obtain acceptable accuracy results which are independent from the accuracy evaluation method used. The error of distorted pixel coordinates is defined as the discrepancy between the real 2D points (u_d, v_d) (obtained from calibration images) and the estimated ones $(\breve{u}_d, \breve{v}_d)$ (obtained by using the camera model). It is given by the following equations:

$$\mathrm{Err} = \frac{\sum_{i=1}^{N} \sqrt{(u_{di} - \breve{u}_{di})^2 + (v_{di} - \breve{v}_{di})^2}}{N} \tag{6}$$

where N is the total number of feature points.

The camera to be calibrated is a consumer-grade camera (ST-423C) with 12 mm lens. The frame size is 720 × 576. The model plane contains a pattern of 6 × 8 chessboard. The size of pattern is 30 mm × 30 mm. It is printed on A4 paper and pasted onto a cardboard. The cardboard is moved and rotated to make captured images cover the most of the field of view. Twenty images of the plane are taken, as shown in Fig. 5.

Table 2 shows the results of camera parameters and calibration accuracy obtained by different methods. From Table 2, it is clear that the proposed method with RANSAC significantly improves the measurement accuracy. The error of distorted pixel coordinates decreases from 0.213 to 0.131 pixel. Furthermore, the NOLIN1 method requires much less iterations than NOLIN2. It occurs in view of the fact that the algorithm NOLIN1 is initialized from the result of the LINEAR1 method, that is closer to the final result, compared to LINEAR2. Evidently this contributes reduces the computational cost of the method.

5. Conclusion

In this paper, we proposed a revisiting 2D calibration method based on RANSAC to evaluate the camera parameters. It is well known that the calibration accuracy mainly depends on the localization of feature points, however it is difficult to accurately and reliably extract all wanted features in all images in the presence of noise, occlusion, image blur, and changing illumination or viewpoint. To address this issue, an effective method is introduced to exclude the unreliable images. First, in our paper, we introduced

the pinhole camera model with lens distortion and demonstrated the basic knowledge of RANSAC. Second, the distance between the circular point and the IAC is defined, which is important in RANSAC and the recommended plane calibration procedure with RANSAC is explained in detail. Furthermore, the recommended threshold value is given by computer simulation. And eventually, we proved the accuracy and robustness of the algorithm by simulation and real experiments. The experimental results show that the proposed method is robust and quite efficient to improve calibration accuracy compared to the traditional methods.

References

[1] Z. Zhang, Y. Han, Y. Zhou, M. Dai, A novel absolute localization estimation of a target with monocular vision, Optik 124 (12) (2013) 1218–1223.
[2] W. Liu, W. Shi, Y. Lv, et al., A novel method of camera pose estimation by parabolic motion, Optik 124 (24) (2013) 6840–6845.
[3] Roger Tsai, A versatile camera calibration technique for high-accuracy 3D machine vision metrology using off the-shelf TV cameras and lenses, IEEE J. Rob. Autom. RA-3 (4) (1987).
[4] Juyang Weng, Paul Cohen, Marc Herniou, Camera calibration with distortion models and accuracy evaluation, IEEE Trans. Pattern Anal. Mach. Intell. 14 (10) (1992) 965–980.
[5] Joaquim Salvi, Xavier Armangue, Joan Batlle, A comparative review of camera calibrating methods with accuracy evaluation, Pattern Recognit. 35 (2002) 1617–1635.
[6] Guangjun Zhang, Junji He, Xianming Yang, Calibrating camera radial distortion with cross-ratio invariability, Opt. Laser Technol. 35 (2003) 457–461.
[7] R. Hartley, A. Zisserman, Multiple View Geometry in Computer Vision, second ed., Cambridge University Press, Cambrige, 2003.
[8] Y. Ma, R. Vidal, J. Kosecka, S. Sastry, Kruppa equation revisited: its renormalization and degeneracy, in: Proceedings of the European Conference on Computer Vision, 2000, pp. 561–577.
[9] S. Maybank, O. Faugeras, A theory of self-calibration of a moving camera, Int. J. Comput. Vision 2 (1992) 123–151.
[10] Guanghui Wang, Hung-Tat Tsui, et al., Camera calibration and 3D reconstruction from a single view based on scene constraints, Image Vision Comput. 23 (2005) 311–323.
[11] B.W. He, Y.F. Li, Camera calibration from vanishing points in a vision system, Opt. Laser Technol. 3 (2008) 555–561.
[12] Z. Zhang, A flexible new technique for camera calibration, IEEE Trans. Pattern Anal. Mach. Intell. 22 (11) (2000) 1330–1334.
[13] J. Heikkila, Geometric camera calibration using circular control points, IEEE Trans. Pattern Anal. Mach. Intell. 22 (2000) 1066–1077.
[14] Z. Zhang, Camera calibration with one-dimensional objects, IEEE Trans. Pattern Anal. Mach. Intell. 26 (7) (2004) 892–899.
[15] F. Qi, Q. Li, Y. Luo, D. Hu, Constraints on general motions for camera calibration with one dimensional objects, Pattern Recognit. 40 (6) (2007) 1785–1792.
[16] José A. de França, R. Marcelo, Stemmer, et al., Revisiting Zhang's 1D calibration algorithm, Pattern Recognit. 43 (2010) 1180–1187.
[17] José A. de França, Marcelo R. Stemmer, et al., A new robust algorithmic for multi-camera calibration with a 1D object under general motions without prior knowledge of any camera intrinsic parameter, Pattern Recognit. 45 (2012) 3636–3647.
[18] Jean-Yves Bouguet, Camera calibration toolbox for Matlab. MRL-Intel Corp., 2004, [online].
[19] Open CV, Open source computer vision library. MRL-Intel Corp., 2008, [online].
[20] Jianbo Su, Camera calibration based on receptive fields, Pattern Recognit. 40 (2007) 2837–2845.
[21] Koen Douterloigne, Werner Goeman, et al., Automatic detection of a one dimensional ranging pole for robust external camera calibration in mobile mapping, ISPRS J. Photogramm. Remote Sens. 86 (2013) 111–123.
[22] Zhen Liu, Xinguo Wei, Guangjun Zhang, External parameter calibration of widely distributed vision sensors with non-overlapping fields of view, Opt. Lasers Eng. 51 (2013) 643–650.
[23] Jun Chu, Anzheng GuoLu, Lu Wang, Chessboard corner detection under image physical coordinate, Opt. Laser Technol. 48 (2013) 599–605.
[24] Stuart Bennett, Joan Lasenby, ChESS-quick and robust detection of chess-board features, Comput. Vision Image Understanding 118 (2014) 197–210.
[25] Junpeng Xue, Xianyu Su, et al., Using concentric circles and wedge grating for camera calibration, Appl. Opt. 51 (17) (2012) 3811–3816.
[26] Guang Jiang, Long Quan, Detection of concentric circles for camera calibration, in: ICCV, 2005, pp. 333–340.
[27] D. Douxchamps, K. Chihara, High-accuracy and robust localization of large control markers for geometric camera calibration, IEEE Trans. Pattern Anal. Mach. Intell. 31 (2) (2009) 376–383.
[28] Ankur Datta, Jun-Sik Kim, et al., Accurate camera calibration using iterative refinement of control points, in: ICCV, 2009, pp. 1201–1208.
[29] Fuqiang Zhou, Yi Cui, et al., A novel optimization method of camera parameters used for vision measurement, Opt. Laser Technol. 44 (2012) 1840–1849.
[30] Fuqiang Zhou, Yi Cui, et al., Accurate and robust estimation of camera parameters using RANSAC, Opt. Lasers Eng. 51 (2013) 197–212.
[31] C. Muruganantham, N. Jawahar, et al., Optimal settings for vision camera calibration, Int. J. Adv. Manuf. Technol. 42 (2009) 736–748.
[32] Carlos Ricolfe-Viala, Antonio Jose, Sanchez Salmeron, Camera calibration under optimal conditions, Opt. Express 19 (11) (2011) 10769–10775.
[33] D.C. Brown, Close-range camera calibration, Photogramm. Eng. 37 (8) (1971) 855–866.
[34] Dapeng Gao, Fuliang Yin, Computing a complete camera lens distortion model by planar homography, Opt. Laser Technol. 49 (2013) 95–107.
[35] M.A. Fischler, R.C. Bolles, Random sample consensus: a paradigm for model fitting with applications to image analysis and automated cartography, Commun. ACM 24 (1981) 381–395.
[36] Krystian Mikolajczyk, Cordelia Schmid, Scale & affine invariant interest point detectors, Int. J. Comput. Vision 60 (1) (2004) 63–86.
[37] Peter Kovesi, Peter's Functions for Computer Vision. CET-University of Western Australia, 2010, [Online].
[38] Fuqiang Zhou, Yi Cui, et al., Line-based camera calibration with lens distortion correction from a single image, Opt. Lasers Eng. 51 (2013) 1332–1343.